






Research on power-frequency electromagnetic interference model of multicore twisted signal cable of high-speed railway

Bowen ZHANG¹, Jiangjian XIE^{1*}, Zhixin WANG^{2,3}, Jin YANG^{2,3}, Hao YAN¹

¹School of Technology, Beijing Forestry University, Beijing, P.R. China

²Beijing National Railway Research & Design Institute of Signal & Communication Co. Ltd, Beijing, P.R. China

³Beijing High-speed Railway Operation Control System Engineering Technology Research Center, Beijing, P.R. China

Received: 13.12.2017

Accepted/Published Online: 03.04.2018

Final Version: 27.07.2018

Abstract: With the increase in the traction power of high-speed railways, the power-frequency electromagnetic interference of traction current to the signal cables becomes increasingly more severe. In this paper, the calculation model of the magnetic interference to signal cable was established on the MATLAB/Simulink platform based on the multi-conductor transmission line theory. This model took SPTYWPL03-8B 8-core twist signal cable as an example and the power-frequency interference of external current to the signal cable was analyzed theoretically. In addition, experiments on electromagnetic interference of double-ended and single-ended signal cables were performed to validate the simulation model. Experiments showed that the relative error was less than 5% by comparing the experimental and simulation results. This research is helpful for the quantitative analysis of the power-frequency electromagnetic interference of traction current to signal cables.

Key words: High-speed railway, signal cable, power-frequency electromagnetic interference, modeling

1. Introduction

With the increase of traction power and the rise of traction return flows, the interference of traction current to signal cables is becoming more and more serious, even leading to the burn-down of signal cables many times in China [1]. To ensure the reliability of signal cables in high-speed railway, it is of great significance to quantitatively investigate the magnetic interference of the power-frequency traction current to signal cables.

At present, the most widely utilized method to analyze electromagnetic interference of traction power supply systems to signal cables is proposed by the International Telegraph and Telephone Consultative Committee. In this method, the cable model is simplified by introducing the shielding coefficient [2–5]. The value of the shielding coefficient was proven to have direct impacts on the accuracy of calculation processes. In practical applications, the shielding coefficients vary from structure to structure, such as the change of the shielding structure and so on [6], and thus using empirical values would certainly cause errors [7]. Therefore, it is arguably necessary to establish the calculation model according to the internal structure of the signal cable.

Calculation models of twisted pair cables have been studied over the past decades. Paul and McKnight [8, 9] analyzed the interference of twisted pair cables by using the theory of cascade transmission lines. Jullien et al. [10] proposed a novel method to equalize a twisted periodic into four uniform transmission lines. The above

*Correspondence: shyneforce@bjfu.edu.cn

model was only applicable to the load for linear cases. With the help of the finite element software ANSYS, Yi and Wang [11] analyzed the electromagnetic field distribution around the double core shielding cable and obtained the calculation parameters of the cable by calculating the charge and flux linkages. In [12], the cable parameters of single twist cycle length were calculated first and then the time domain equivalent broadband model of multitwisted cable was deduced based on multiconductor transmission line (MTL) theory. Brink et al. [13] elaborated on a full 8-port model of twisted pair quad cables to quantify various characteristics of this dual slope behavior of in-quad EL-FEXT. Armenta et al. [14] modeled the twisted-wire pair bundles as a cascade of electrically short uniform transmission-line sections rotated continuously in radio frequency. Under the condition of power frequency, twisted wires can be approximately equivalent to parallel multiconductor transmission lines [15]. Based on this premise, we can propose a simplified model of multicore twisted signal cables to improve the computational efficiency.

In this paper, we took the 8-core twisted cable SPTYWPL03-8B as an example, which is commonly used in high-speed railways, and deduced the model of multicore twisted signal cables under power frequency based on parallel multiconductor transmission line theory. We then analyzed the electromagnetic interference of the external current-carrying wires to the signal cable and finally designed electromagnetic interference experiments to validate the proposed models.

2. Simplified model of signal cable under power frequency

2.1. SPTYWPL03-8B railway digital signal cable

The SPTYWPL03-8B cable contains two groups of four star-twisted core wires. The four star-twisted core wires consist of four conductors with the same electrical and geometric parameters, which are twisted clockwise smoothly. Four core wires are covered with copper foil shielding. Twisted cycle length is 200 mm and its structure is shown in Figure 1.

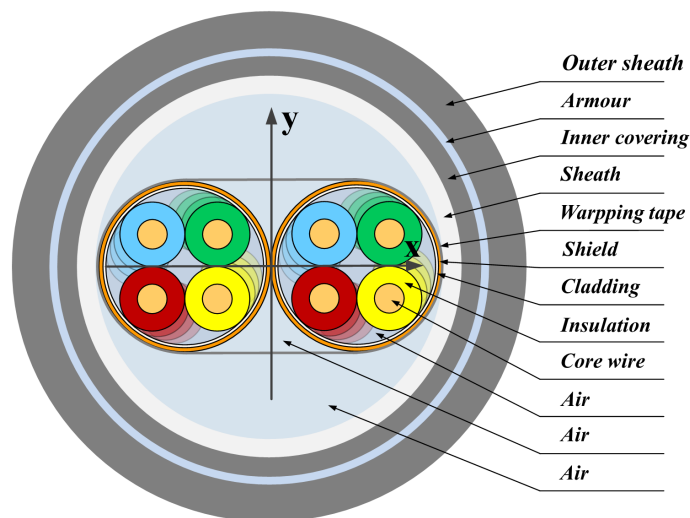


Figure 1. Structure schematic diagram of SPTYWPL03-8B cable.

2.2. Modeling of signal cable

In practical applications, two of the four core wires in each group are often used as backup, and the current directions in other two core wires are opposite. Accordingly, when we consider the interference of the external current-carrying conductor to the core wire, the interference between two groups of four star-twisted core wires can be neglected and only two core wires in one group are left to be considered herein. Then the cable is simplified as a multiconductor transmission line that contains five conductors, two core wires, a sheath layer, a shield layer, and an armor layer where the sheath, shield, and armor layers can be regarded as cylindrical tubular conductors with annular sections under power frequency [16]. Figure 2 shows the sectional view of the simplified cable.

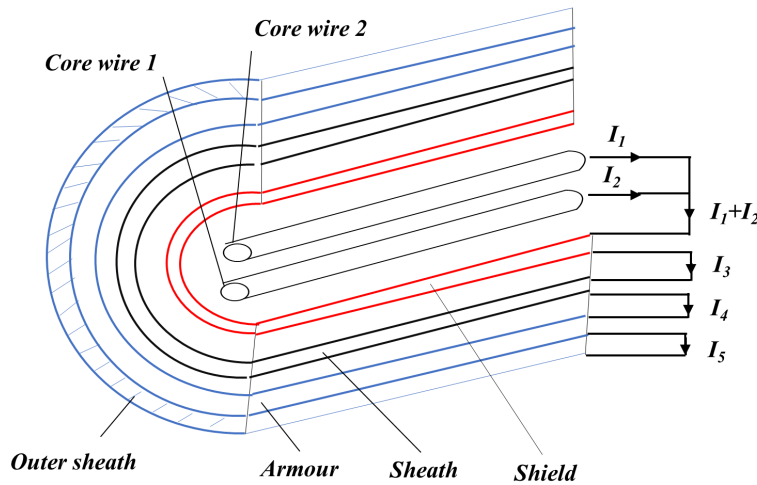


Figure 2. Sectional view of cable.

The loop currents of the two core wires, shield, sheath, and armor layers are I_1 , I_2 , I_3 , I_4 , and I_5 . The current flows through core wire 1, core wire 2, shield, sheath, and armor layers are denoted as I_{1x} , I_{2x} , I_p , I_h , and I_k , respectively. The currents in the shield, sheath, and armor layers are I_p , I_h , and I_k . V_1 , V_2 , V_3 , V_4 , and V_5 are the voltage differences between core wire 1 and the shielding layer, core wire 2 and the shielding layer, the shielding layer and the sheathing layer, the sheathing layer and the sheathing layer, and the sheathing layer and the earth at infinity. V_{1x} , V_{2x} , V_p , V_h , and V_k represent the reference voltages between infinity and the corresponding conductor. The relationship between them is shown as follows.

$$\begin{cases} I_1 = I_{1x} \\ I_2 = I_{2x} \\ I_3 = I_p + I_{1x} + I_{2x} \\ I_4 = I_p + I_{1x} + I_{2x} + I_h \\ I_5 = I_p + I_{1x} + I_{2x} + I_h + I_k \end{cases} \quad (1)$$

$$\begin{cases} V_1 = V_{1x} - V_p \\ V_2 = V_{2x} - V_p \\ V_3 = V_p - V_h \\ V_4 = V_h - V_k \\ V_5 = V_k \end{cases} \quad (2)$$

The following equations can be listed based on the loop voltages and the loop currents.

$$\begin{cases} -\frac{dV_1}{dx} = Z'_{11}I_1 + Z'_{12}I_2 + Z'_{13}I_3 + Z'_{14}I_4 + Z'_{15}I_5 \\ -\frac{dV_2}{dx} = Z'_{21}I_1 + Z'_{22}I_2 + Z'_{23}I_3 + Z'_{24}I_4 + Z'_{25}I_5 \\ -\frac{dV_3}{dx} = Z'_{31}I_1 + Z'_{32}I_2 + Z'_{33}I_3 + Z'_{34}I_4 + Z'_{35}I_5 \\ -\frac{dV_4}{dx} = Z'_{41}I_1 + Z'_{42}I_2 + Z'_{43}I_3 + Z'_{44}I_4 + Z'_{45}I_5 \\ -\frac{dV_5}{dx} = Z'_{51}I_1 + Z'_{52}I_2 + Z'_{53}I_3 + Z'_{54}I_4 + Z'_{55}I_5 \end{cases} \quad (3)$$

Here, the impedance parameter can be calculated by Eq. (4).

$$\begin{cases} Z'_{11} = Z_i + j\omega L_{11} + Z_{p-in} \\ Z'_{12} = Z'_{21} = j\omega L_{12} + Z_{p-in} \\ Z'_{22} = Z_i + j\omega L_{22} + Z_{p-in} \\ Z'_{13} = Z'_{23} = Z'_{32} = Z'_{31} = -Z_{p-mutual} \\ Z'_{33} = Z_{p-out} + Z_{ph-ins} + Z_{h-in} \\ Z'_{14} = Z'_{24} = Z'_{41} = Z'_{42} = 0 \\ Z'_{34} = Z'_{43} = -Z_{h-mutual} \\ Z'_{44} = Z_{h-out} + Z_{hk-ins} + Z_{k-in} \\ Z'_{15} = Z'_{25} = Z'_{51} = Z'_{52} = Z'_{35} = Z'_{53} = 0 \\ Z'_{45} = Z'_{54} = -Z_{k-mutual} \\ Z'_{55} = Z_{k-out} + Z_{kg-ins} + Z_g \end{cases} \quad (4)$$

The internal impedance of the core wire was calculated as follows.

$$Z_i(j\omega) = \frac{1}{\pi\sigma R^2} + \frac{1}{2\pi R} \sqrt{\frac{\mu}{\sigma}} \sqrt{j\omega} \quad (5)$$

Self-inductance and mutual inductance of the core wires, L_{11} , L_{12} , and L_{22} , were calculated by Eqs. (6) and (7) [17].

$$L_{GG,RR} = \frac{\mu_0}{2\pi} \ln\left(\frac{r_{SH}^2 - d_{G,R}^2}{r_{SH}r_{wG,R}}\right) \quad (6)$$

$$L_{GR} = \frac{\mu_0}{2\pi} \ln\left(\frac{d_R}{r_{SH}} \sqrt{\frac{(d_G d_R)^2 + r_{SH}^4 - 2d_G d_R r_{SH}^2 \cos(\theta_{GR})}{(d_G d_R)^2 + d_R^4 - 2d_G d_R^3 \cos(\theta_{GR})}}\right) \quad (7)$$

Here, r_{SH} is the shield radius while r_{WR} is the radius of the core wire. d_R and d_G are the distances between centers of the core wire and shield. θ_{GR} is the angle between the two core wires. Figure 3 shows the layout of the core wire inside the shield.

The tubular conductor can be treated as two transmission lines with internal impedance and external impedance, respectively. Z_{in} is the surface impedance (internal impedance) of the inside reflow current. Z_{out} is the surface impedance of the outside reflow current (external impedance). Z_{mutual} is the transfer resistance (mutual impedance) between the inside and outside surface. With the inner and outer tubular radii being a and b , Wedepohl derived the approximate formula of the tubular conductor impedance when $[(b-a) / (b + a)] < 1/8$ at low frequencies [18].

$$Z_{in} \approx \frac{\sqrt{j\omega\mu\sigma}}{2\pi\sigma a} \coth(\sqrt{j\omega\mu\sigma}(b - a)) - \frac{1}{2\pi\sigma a(a + b)} \quad (8)$$

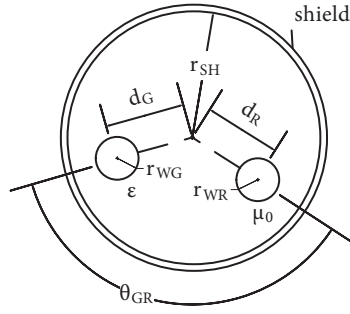


Figure 3. Arrangement diagram of core wire inside the shield.

$$Z_{out} \approx \frac{\sqrt{j\omega\mu\sigma}}{2\pi\sigma b} \coth(\sqrt{j\omega\mu\sigma}(b-a)) - \frac{1}{2\pi\sigma b(a+b)} \quad (9)$$

$$Z_{mutual} \approx \frac{\sqrt{j\omega\mu\sigma}}{\pi\sigma(a+b)} - \frac{1}{\sinh(\sqrt{j\omega\mu\sigma}(b-a))} \quad (10)$$

The formulas listed above were used to calculate the impedance of the shield (Z_{p-in} , Z_{p-out} , $Z_{p-mutual}$), sheath (Z_{h-in} , Z_{h-out} , $Z_{h-mutual}$), and armor (Z_{k-in} , Z_{k-out} , $Z_{k-mutual}$). The inductance of the insulation layer can be calculated by Eq. (11).

$$L_{ins} = \frac{\mu_0}{2\pi} \ln\left(\frac{b}{a}\right) \quad (11)$$

Here, a and b are inner and outer radius of the insulation layer respectively. Ground impedance was calculated by Theethayi's approximate formula [19], which is shown as Eq. (12).

$$Z_g = \frac{j\omega\mu_0}{2\pi} \left(\ln\left(\frac{\gamma_g R + 1}{\gamma_g R}\right) + \frac{2}{4 + \gamma_g^2 R^2} e^{-2d|\gamma_g|} \right) \quad (12)$$

Here, the propagation constant γ_g is as follows.

$$\gamma_g = \sqrt{j\omega\mu_0(\sigma_g + j\omega\epsilon_g)} \quad (13)$$

By substituting Eqs. (1) and (2) into Eq. (3), the corresponding MTL equation was deduced:

$$-\frac{d}{dx} \begin{bmatrix} V_{1x} \\ V_{2x} \\ V_p \\ V_h \\ V_k \end{bmatrix} = [Z] \begin{bmatrix} I_{1x} \\ I_{2x} \\ I_p \\ I_h \\ I_k \end{bmatrix} \quad (14)$$

This is the impedance matrix of the MTL.

By solving the MTL of Eq. (14), calculation results can be used to analyze the coupling phenomenon between the metal epidermis (including the shield, sheath, and armor) and the inner core. In MATLAB/Simulink, we can use the Mutual Inductance block to build the signal cable model.

3. Electromagnetic interference of the external current-carrying conductor to the signal cable

Electromagnetic interference of the external current-carrying conductor to the signal cable core can be divided into two parts. The first part is caused by capacitive couple while the other is caused by inductive couple. Considering the presence of grounding points, the capacitive couplings of both single-ended and double-ended grounding mode were neglected. In this paper, only inductive coupling was considered.

3.1. Theoretical analysis of interference

We simplified the traction power supply system into two external current-carrying conductors, namely the contact wire and the ground wire, and only one core wire was considered. The metal epidermis of the signal cable was grounded with the ground wire. Induced voltage of the core wire was produced by the inductive coupling of the contact wire, the ground wire, and the metal epidermis. We consider 1 km of the signal cable; Figure 4 shows the equivalent circuit of the interference model.

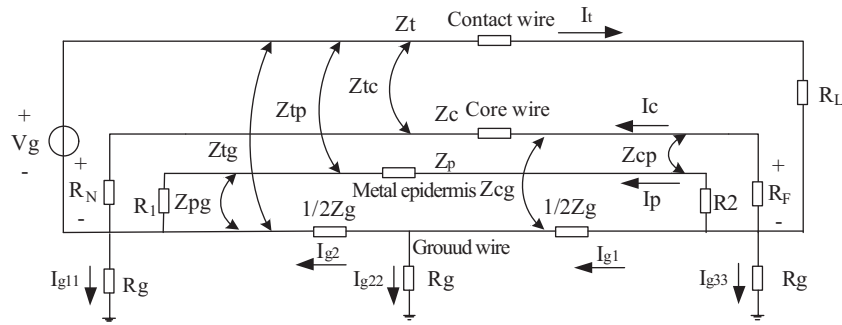


Figure 4. Equivalent circuit of interference model.

By changing the resistance values of R_1 and R_2 , we can simulate single-ended and double-ended grounding modes. The meanings of Z_t , Z_c , Z_p , Z_g , R_g , Z_{tc} , Z_{tp} , Z_{tg} , Z_{cp} , Z_{cg} , and Z_{pg} are listed in Table 1. I_t , I_c , I_p , I_{g1} , and I_{g2} denote the currents flowing through the contact wire, core wires, shield, and ground wire, respectively. I_{g11} , I_{g22} , and I_{g33} are leakage currents of the ground wire to the ground.

The following voltage equations were deduced by using Kirchoff's voltage law:

$$-V_g + (R_L + Z_t)I_t - (Z_{tc}I_c + Z_{tp}I_p + \frac{1}{2}Z_{tg}(I_{g1} + I_{g2})) + R_g I_{g33} - R_g I_{g11} = 0 \quad (15)$$

$$(Z_c + R_N + R_F)I_c + (-Z_{tc}I_t + Z_{cp}I_p + \frac{1}{2}Z_{cg}(I_{g1} + I_{g2})) - R_g I_{g33} + R_g I_{g11} = 0 \quad (16)$$

$$(Z_p + R_1 + R_2)I_p + (-Z_{tp}I_t + Z_{cp}I_c + \frac{1}{2}Z_{pg}(I_{g1} + I_{g2})) - R_g I_{g33} + R_g I_{g11} = 0 \quad (17)$$

$$\frac{1}{2}Z_g(I_{g1} + I_{g2}) + (-Z_{tg}I_t + Z_{cg}I_c + Z_{pg}I_p) - R_g I_{g33} + R_g I_{g11} = 0 \quad (18)$$

$$\frac{1}{2}Z_g I_{g1} - R_g I_{g33} + R_g I_{g22} + \frac{1}{2}(-Z_{tg}I_t + Z_{cg}I_c + Z_{pg}I_p) = 0 \quad (19)$$

The following current equations were obtained using Kirchhoff’s current law:

$$I_t=I_c + I_p + I_{g1} + I_{g33} \tag{20}$$

$$I_t=I_c + I_p + I_{g2} - I_{g11} \tag{21}$$

$$I_{g1}=I_{g2} + I_{g22} \tag{22}$$

By solving Eqs. (15)-(22), we can obtain the currents in each wire and the voltages in each node, and then we can obtain the induced voltage in the core wire.

3.2. Simulation of the interference

With the simplified interference model in Figure 4, we established the corresponding simulation model. From top to bottom, the Mutual Inductance block presents the contact wire, the core wire, the metal epidermis, and the ground wire, respectively. With the calculation parameters (in Table 1), we obtain the currents of all wires by the theoretical calculation in Section 3.1. The corresponding results were calculated by simulation. Table 2 presents the comparison between them. The results of the simulation and the theoretical calculation are nearly the same, which validates the accuracy of the simulation model.

Table 1. Calculation parameters.

| Parameter (unit) | Value |
|---|----------------|
| Contact wire-earth loop impedance Z_T (Ω/km) | 0.1353+0.6561i |
| Core wire-earth loop impedance Z_C (Ω/km) | 0.27+0.95i |
| Metal epidermis-earth loop impedance Z_P (Ω/km) | 0.5612+0.0963i |
| Ground wire-earth loop impedance Z_g (Ω/km) | 0.7763+0.9527i |
| Mutual impedance between contact wire and core wire Z_{TC} (Ω/km) | 0.0493+0.2967i |
| Mutual impedance between contact wire and metal epidermis Z_{TP} (Ω/km) | 0.0493+0.2967i |
| Mutual impedance between contact wire and the ground wire Z_{TG} (Ω/km) | 0.0492+0.3791i |
| Mutual impedance between core wire and metal epidermis Z_{CP} (Ω/km) | 0.5519+0.0354i |
| Mutual impedance between core wire and the ground wire Z_{CG} (Ω/km) | 0.0493+0.6614i |
| Mutual impedance between ground wire and metal epidermis Z_{PG} (Ω/km) | 0.0493+0.6614i |
| Voltage of traction system V_g (V) | 27500 |
| Rail-to-ground resistance R_g (Ω) | 1.93e6–1.13e5i |
| $R_N=R_F$ (Ω) | 1e12 |
| $R_1=R_2$ (Ω) | 0 |

We set $R_1=R_2=0$ and $R_1=1e12$, $R_2=0$, to simulate double-ended and single-ended grounding mode, respectively. The induced voltages of the core wire under different grounding modes were obtained by simulation and the results are shown in Table 3.

The induced voltage of the double-ended mode is higher than that of the single-ended mode. The reason is that the double-ended grounding is equivalent to parallel shunting of the ground wire and the metal epidermis, so the metal epidermis has a larger current, causing higher induced voltage. Under this condition, the burn-down phenomenon of the metal epidermis may easily occur.

Table 2. Comparison between simulation and theory calculation.

| Parameter | Theoretical calculation | Simulation | Relative error of amplitude |
|-----------|-------------------------|------------|-----------------------------|
| I_t | 775.222 | 775.222 | 0.00% |
| I_c | 2.381e-10 | 2.38e-10 | -0.09% |
| I_p | 676.214 | 676.287 | 0.01% |
| I_{g1} | 223.978 | 223.799 | -0.08% |
| I_{g2} | 223.978 | 223.799 | -0.08% |
| I_{g11} | 8.581e-05 | 8.57e-05 | -0.10% |
| I_{g22} | 0 | 1.91e-13 | 0.00% |
| I_{g33} | 8.581e-05 | 8.57e-05 | -0.10% |

Table 3. Comparison of induced voltage of core wire under different grounding modes.

| Grounding mode | Induced voltage (V) |
|----------------|---------------------|
| Single-ended | 139.988 |
| Double-ended | 155.128 |

4. Power-frequency electromagnetic interference experiment

We performed an electromagnetic interference experiment of the cable to verify the accuracy of the proposed simulation model. The experimental arrangement is shown in Figure 5. An SPTYWPL03-8B cable with length of 330 m was laid along the interior wall of a factory warehouse.

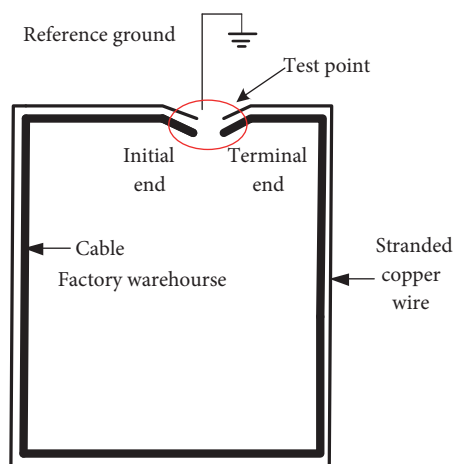


Figure 5. Experimental arrangement.

An input of 220 V voltage and rated capacity of 3 kVA voltage regulator were used for the power-frequency source. A 20 Ω current limiting resistor was used to limit the current. The source and test equipment were set at the end of the cable, and the reference ground of measurement was set at a place 20 m away from the test area. A 25 mm² stranded copper wire was set along the signal cable to simulate the ground wire. An oscilloscope was used to measure the voltage waveform between both ends of the core wire.

4.1. Interference test of double-ended grounding cable

In the double-ended grounding mode, the metal epidermis and the ground wire are equivalent to be parallel connected. To simplify the test, the power-frequency source was connected to both ends of the metal epidermis. The test wiring is shown in Figure 6.

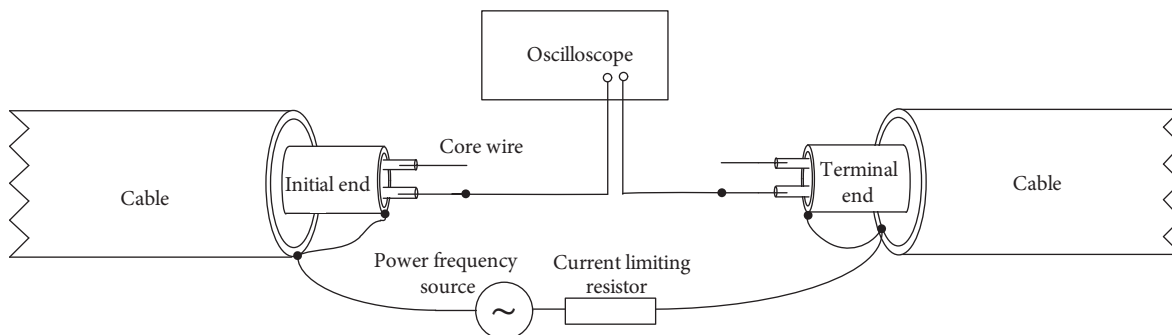


Figure 6. Wiring diagram of test of double-ended grounding of cable.

By adjusting the voltage regulator and changing the currents to 5 A, 8 A, and 10 A, respectively, we performed the experiment with each current value four times. The average power-frequency induced voltage amplitude of the core wire under different currents are shown in Table 4. The comparison of simulation and test results are listed in Table 4. The relative errors of amplitude are less than 5%, which means that the simulation results match the test results well.

Table 4. Induced voltage amplitude comparison of core wire.

| Current (A) | Test (V) | Simulation (V) | Relative errors of amplitude |
|-------------|----------|----------------|------------------------------|
| 5 | 3.195 | 3.118 | 2.410% |
| 8 | 4.940 | 4.972 | 0.648% |
| 10 | 6.483 | 6.216 | -4.118% |

4.2. Interference test of single-ended grounding cable

Under the single-ended grounding mode, current only flows through the ground wire. The test wiring is shown in Figure 7. The ground wire was connected to the metal epidermis only at the initial end. The power-frequency source was connected to both ends of the ground wire.

When the currents in ground wires were 5 A and 8 A, the measured induced voltage values are too small to recognize since they were submerged by external noises. The induced voltage amplitude is 2 V when the current value is 10 A, the induced voltage amplitude of simulation is 1.996 V, and relative error is 0.2%, and the simulation results match the test results well, too.

5. Conclusion

In this paper, we established a power-frequency interference model of multicore twisted cable based on multi-conductor transmission theory. With this model, we analyzed the electromagnetic interference of an external current-carrying conductor to the signal cable under different grounding modes and performed electromagnetic interference experiments. The relative error rates of the test results and simulation results were less than 5%,

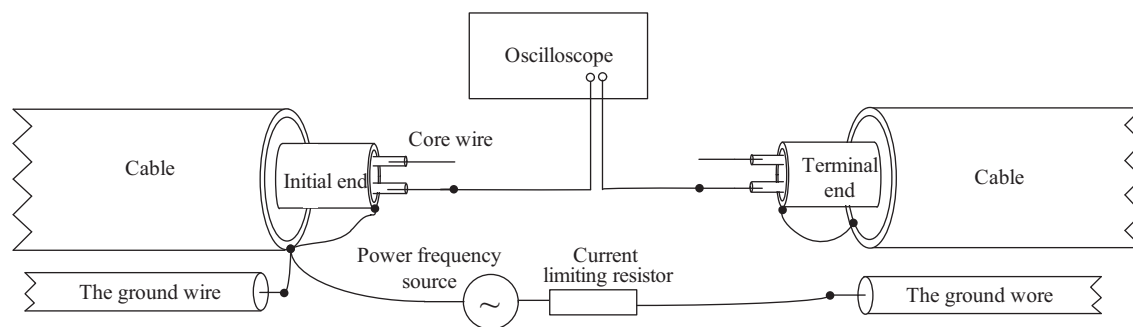


Figure 7. Wiring diagram of test of single-ended grounding of cable.

which validated the accuracy of the proposed model. In the future, by means of combining this model with the simulation model of a traction power supply system, we can analyze the interference of the traction power supply system to the signal cable more accurately and provide a theoretical basis for the protection of signal cables.

Acknowledgment

The paper was supported by the Fundamental Research Funds for the Central Universities (No. 2017JC14 & No. 2016ZCQ08).

References

- [1] Editorial Board of Daqin Heavy Haul Railway Service Technology and Application. Daqin Heavy-haul Railway Power Technology and Application. Beijing, China: China Railway Publishing House, 2009 (in Chinese).
- [2] Xiao XJ. Analysis and calculation of electromagnetic influence on railway electrification and development of its software system. PhD, Central South University, Changsha, China, 2005 (in Chinese).
- [3] Chang YY. Study on some problems of the effect of high-speed railway traction power supply system on the electromagnetic of signal cables. PhD, China Railway Academy, Beijing, China, 2011 (in Chinese).
- [4] Xu YH. Research on the influence of passenger traction current on the signal cable electromagnetism. PhD, Lanzhou Jiaotong University, Lanzhou, China, 2013 (in Chinese).
- [5] Yang SW, Zhang X, Liang MY, Wang JH. Research on grounding method and longitudinal electromotive force test of railway signal cable. *J Instrum* 2013; 34: 254-259.
- [6] Colak B, Cerezci O, Ari N, Helhel S. Optimization of shielding effectiveness of coaxial double braided screens in contact. In: *IEEE 2016 9th International Kharkiv Symposium on Physics and Engineering of Microwaves, Millimeter and Submillimeter Waves*; 20–24 June 2016; Kharkiv, Ukraine. New York, NY, USA: IEEE. pp. 1-3.
- [7] Mariscotti A. Induced voltage calculation in electric traction systems: simplified methods, screening factors, and accuracy. *IEEE T Intell Transp* 2011; 12: 201-210.
- [8] Paul CR, McKnight JW. Prediction of crosstalk involving twisted pairs of wires-Part II: A simplified low-frequency prediction model. *IEEE T Electromagn C* 2007; 21: 105-114.
- [9] Paul CR, McKnight JW. Prediction of crosstalk involving twisted pairs of wires-Part I: A transmission-line model for twisted-wire pairs. *IEEE T Electromagn C* 2007; 21: 92-105.
- [10] Jullien C, Besnier P, Dunand M, Junqua I. Advanced modeling of crosstalk between an unshielded twisted pair cable and an unshielded wire above a ground plane. *IEEE T Electromagn C* 2013; 55: 183-194.

- [11] Yi B, Wang ZZ. Calculation of shielded cable parameters and crosstalk between the shield and the core. *High Voltage Technology* 2008; 34: 804-808.
- [12] Xiang NW, Chen WJ, Li CR, Chen JH, Gu SQ, Xu ZQ. Research on wide band modeling of high-speed railway signal system multi-core twisted cable. *Journal of Chinese Electrical Engineering* 2016; 36:554-562.
- [13] Brink RFMVD. Modeling the dual-slope behavior of in-quad EL-FEXT in twisted pair quad cables. *IEEE T Commun* 2017; 65: 2153-2163.
- [14] Armenta RB, Sarris CD. Modeling of plane-wave incidence on a twisted-wire pair bundle for RF ingress estimation in digital subscriber line systems. In: *IEEE 2006 12th International Symposium on Antenna Technology and Applied Electromagnetics and Canadian Radio Sciences Conference*; 17–19 July 2006; Montreal, Canada. New York, NY, USA: IEEE. pp. 1-4.
- [15] Li X. Research on crosstalk of multi-strand based on multi-conductor transmission line theory. PhD, Jilin University, Changchun, China, 2009 (in Chinese).
- [16] Rachidi F, Tkachenko S. *Electromagnetic Field Interaction with Transmission Lines. From Classical Theory to HF Radiation Effects*. Ashurst, UK: WIT Press, 2013.
- [17] Paul CR. Introduction to electromagnetic compatibility (EMC). *IEE Rev* 2006; 38: 1-12.
- [18] Wedepohl LM, Wilcox DJ. Transient analysis of underground power-transmission systems. System-model and wave-propagation characteristics. *P IEE* 1973; 120: 253-260.
- [19] Theethayi N, Thottappillil R, Paolone M, Nucci CA. External impedance and admittance of buried horizontal wires for transient studies using transmission line analysis. *IEEE T Dielect El In* 2007; 14: 751-761.